5-2022

Addressing the Performance of Distance Relays in Presence of Inverter Based Resources

Prabin Adhikari
prabina@clemson.edu

ADDRESSING THE PERFORMANCE OF DISTANCE RELAYS IN PRESENCE OF INVERTER BASED RESOURCES

A Thesis
Presented to
the Graduate School of
Clemson University

In Partial Fulfillment
of the Requirements for the Degree
Master of Science
Electrical Engineering

---

by
Prabin Adhikari
May 2022

Accepted by:
Dr. Sukumar Brahma, Committee Chair
Dr. Johan Enslin
Dr. Ramtin Hadidi

Abstract

The transition towards clean energy initiatives to reduce global greenhouse emissions and the dependence on fossil fuels requires the interconnection of large-scale renewable energy power plants (REPPs) to high voltage transmission networks via inverters. These inverter interfaced power sources, popularly known as inverter-based resources (IBRs), pose several technical challenges to the existing distance protection infrastructures widely deployed in transmission systems.

Fault characteristics of IBRs are significantly different from those shown by synchronous generators (SGs). With IBRs taking a large share of generation, their increasing penetration at the transmission level causes incorrect operation of existing distance protection schemes designed for systems dominated by SGs. This work focuses on the impact of inverters on negative sequence component-based directional elements that assist distance relays in identifying the direction of fault current, causing incorrect tripping of relays and missing out on in-zone faults. The main reasons for these misoperations are the negative sequence current blocking function in inverters and the changed angular relationships between the sequence voltages and currents dictated by the IBR control schemes.

This work proposes a solution that uses the method of fault direction identification used in classical non-numerical relays to address this problem. Unlike modern numerical relays, directional elements in non-numerical relays use the measurements of phase voltages and currents instead of negative sequence components. This work shows that the method of direction identification used by non-numerical relays still works accurately in all test scenarios, including cases with IBR feeding the relay, where the negative sequence component-based method in modern numerical relays fails.

Acknowledgements

I want to express my sincere gratitude to my advisor Dr. Sukumar Brahma for his expert guidance, support, and encouragement throughout my M.S. thesis research. This work would not have been possible without his supervision.

I am incredibly thankful to my advising committee members— Dr. Johan H. Enslin and Dr. Ramtin Hadidi, for their constructive comments and generous support. Their feedback has always shown me the right research direction and motivated me to become a better student. I appreciate the feedback and motivation offered by my labmates Phani Harsha Gadde, Trupal Patel, and Munim Bin Gani. Discussions with them have always been insightful with valuable comments.

This work was supported by two awards by the U.S. Department of Energy's Office of Energy Efficiency and Renewable Energy(EERE) under the Solar Energy Technologies Office Sandia National Laboratories. First, through Sandia National Laboratories by Agreement Number 36533 - subaward to Clemson University, and second, through the University of North Carolina, Charlotte by Award Number DE-EE0008774, subaward 20190382-01-CLE. Sandia National Laboratories is a multi-mission laboratory managed and operated by National Technology and Engineering Solutions of Sandia, LLC, a wholly-owned subsidiary of Honeywell International Inc., for the U.S. Department of Energy's National Nuclear Security Administration under contract DE-NA0003525.

Contents

Section **Page**

Title Page **i**

Abstract **ii**

Acknowledgements **iii**

Contents **iv**

List of Figures **vi**

List of Tables **viii**

Nomenclature **ix**

---

1 Introduction and Literature Review **1**

1.1 Penetration of inverter based resources in transmission grids 3

1.2 IBR impacts on distance relay 4

1.3 Distance protection with IBRs literature review 6

1.4 Organization of thesis 8

---

2 Inverter Modeling and Control **9**

2.1 Overview of the model 9
2.2 Control system 9
2.2.1 Normal operating condition 10
2.2.2 Abnormal operating condition 11

3 Distance Relays **14**
3.1 Non-numerical distance relays 16
3.2 Numerical distance relays 18

4 Simulation Test System **22**
4.1 Transmission line 23
4.2 Synchronous generators 23
4.3 IBR 24
4.4 Distance relays 24

5 Results and Discussion **25**
5.1 Fault characteristics of inverter model 26
5.2 Performance of relays when fed by SG 27
5.3 Performance of relays when fed by IBR 28

6 Conclusion **34**

List of Figures

Figure **Page**

1.1 States in the US with their RPS status [3]. 2

1.2 Anticipated energy mix in the US [4]. 3

1.3 Anticipated renewable energy mix in the US [4]. 3

2.1 Overall control schematic of the inverter model. 10

2.2 Siemens-Gamesa control logic for FRT implementation. 11

3.1 Working principle of 90° - 30° directional element. 17

3.2 Negative sequence circuit of a transmission system. 19

3.3 Working principle of 67Q directional element. 21

4.1 Simulation test system with SG behind the distance relay. 22

4.2 Simulation test system with an IBR behind the distance relay. 24

5.1 IBR performance for an AG fault. 27

5.2 IBR performance for a BCG fault. 27

5.3 Recording by a numerical relay during an AG fault fed by a SG. . . . 29

5.4 Recording by an electromechanical relay during an AG fault fed by a SG. 29

5.5 Magnitude of negative sequence currents during an AG fault with different sources. 30

5.6 Recording by a numerical relay during an AG fault fed by an IBR. . . 30
5.7 Recording by an electromechanical relay during an AG fault fed by an IBR. 31
5.8 Phase a current magnitude during an AG fault with different sources 31

List of Tables

Table **Page**

3.1 Distance relay units and their inputs 15

5.1 Comparison of the performance of relays with SG 30

5.2 Comparison of the performance of relays with IBRs 32

Nomenclature

IBR	-	Inverter Based Resource
SG	-	Synchronous Generator
RE	-	Renewable Energy
RPS	-	Renewable Portfolio Standard
FRT	-	Fault Ride Through
FID	-	Fault type Identification
PCC	-	Point of Common Coupling
PLL	-	Phase Locked Loop
DSC	-	Delayed Signal Cancellation
PWM	-	Pulse Width Modulation
MTA	-	Maximum Torque Angle
LG	-	Line-to-Ground
LL	-	Line-to-Line
LLG	-	Line-to-Line-to-Ground

Chapter 1

Introduction and Literature Review

Significant efforts are being made worldwide to tackle the impacts of climate change: the US recently rejoined the Paris agreement with strengthened targets of reducing emissions by more than 50% below 2005 levels by 2030 [1], and the European Commission has a target of reducing the greenhouse emissions by 40-45% by 2030 below 1990 levels [2]. With these goals, there have been continuous efforts to reduce the dependency on fossil fuel-based energy sources and promote renewable energy (RE) sources. Currently, thirty states in the US have renewable portfolio standard (RPS) policies that require at least some percentage of the retail load to be supplied via RE sources. Moreover, several states including Arizona, Washington DC, Hawaii, and Washington, have raised their RPS target to 100% before 2050 [3]. The present status of RPS in different states of the US is shown in Figure 1.1. Having target goals for RPS has played a crucial role in increasing the growth of RE in many states.

As the world moves forward with clean energy initiatives, energy generation using RE

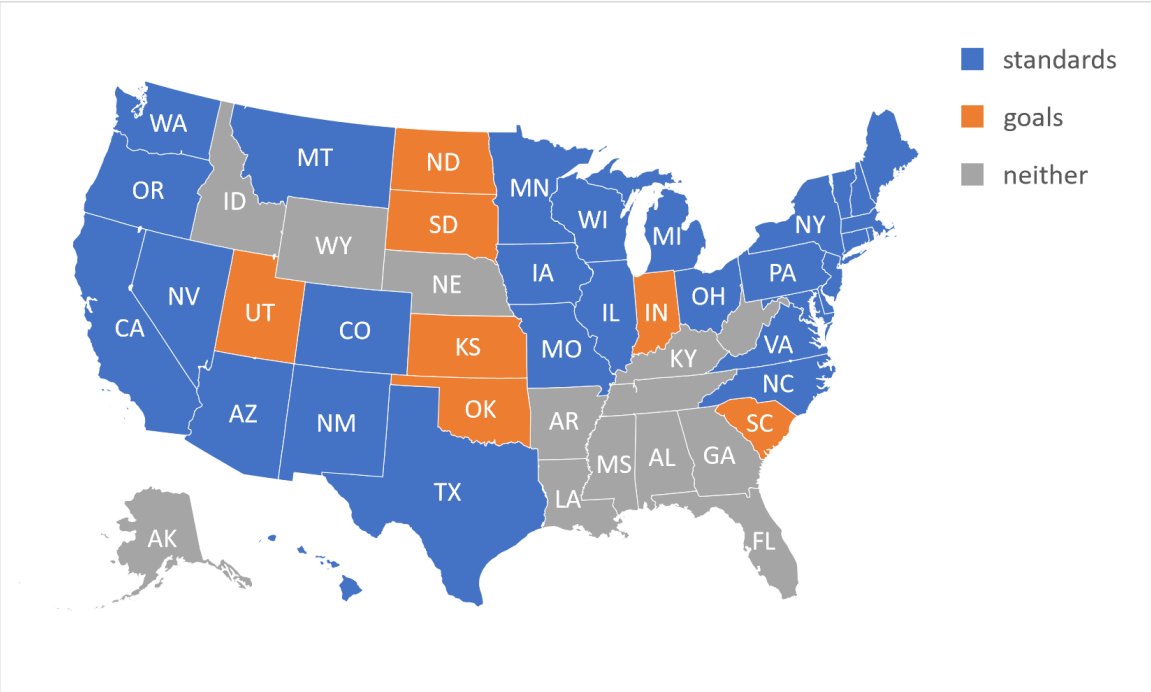

Figure 1.1: States in the US with their RPS status [3].

sources is expected to grow over the next few decades. This increase will be abetted by continuous evolution in RE technology and power electronics. Figure 1.2 shows the projected energy mix in the US up to 2050; a fair share of the generation mix (42%) is expected to be taken by renewables by that time. Also, the generation from solar and wind energy is projected to have a significant proportion (81% combined) of the total renewable energy generation as depicted in Figure 1.3. These large-scale RE sources are centralized. Transmission of bulk power generated requires them to be interfaced to the high voltage ac transmission networks through inverters. Increasing penetration of inverter based resources (IBRs) into transmission systems poses power system operators and researchers with the challenge of keeping the grid safe and resilient, since their behavior in steady state and disturbed state is significantly different than the conventional synchronous generators.

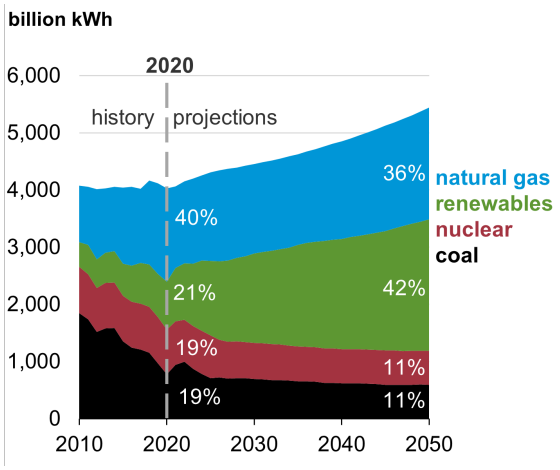

Figure 1.2: Anticipated energy mix in the US [4].

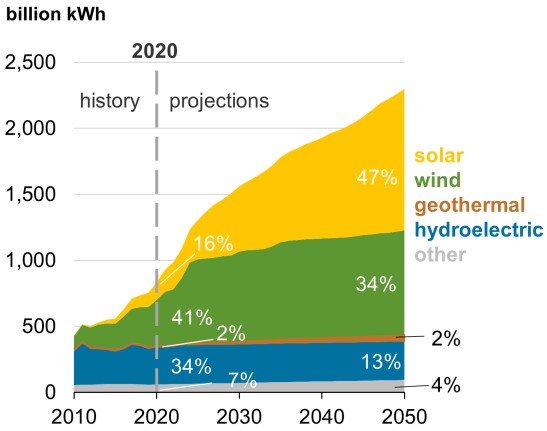

Figure 1.3: Anticipated renewable energy mix in the US [4].

1.1 Penetration of inverter based resources in transmission grids

Existing transmission grids are mostly designed to operate with conventional sources like SGs. Unlike conventional energy sources, generation from IBRs suffers from issues like unpredictability and variability. As large-scale IBRs replace conventional fuel-based energy sources, it becomes essential to study the potential challenges associated with this integration. Integration of large-scale RE sources via inverters poses several technical challenges to the existing grids, especially during extreme events like faults when grid voltage support is impaired.

To address these challenges, grids hosting IBRs have grid codes as standards that dictate the behavior of IBRs during extreme events like faults. These standards have requirements like fault-ride through (FRT), active power and frequency control, reactive power and voltage control, maintaining specific voltage and frequency boundaries [5]. Grid codes [6, 7] specifically require IBRs to have reactive power injection priority during faults by controlling the power factor of the fault current, depending on the terminal voltage. Furthermore, power electronics components of

inverters are susceptible to thermal damage due to currents higher than their rated current. As a result, fault current contribution from IBRs is limited to 1.1 to 1.5 pu of its rating. In addition to these requirements, the fault current contribution from IBRs is purely positive sequence, and they are controlled to block negative sequence currents [8]. These control schemes and physical limitations of IBRs make their fault characteristics significantly different from those of conventional SGs.

1.2 IBR impacts on distance relay

Distance relays measure the positive sequence impedance to the fault from the measurement point and operate if the measured impedance is within the set range. The distance protection scheme is extensively used for the protection of transmission lines as their protection range and sensitivity are robust to system operating conditions [9]. The functional design of distance relays stems from the assumption of the system being fed by SGs. Fault signatures of SGs are well known and modeled by a linear Thevenin model. Similar characterization is not possible for IBRs as their response to fault is nonlinear and varies with make and model [10]. Therefore, when IBRs replace SGs within the existing transmission system, distance protection is compromised [11].

Distance relays mainly consist of distance, directional, and fault type identification (FID) elements. Distance element measures the positive sequence impedance to the fault. Directional element assists distance relay with identifying the direction of fault current. Fault type classification is done by the FID element of the distance relay. Failure in any one of these elements affects the performance of the distance relay. Published literature has discussed the impact of IBRs on each of these elements. Fang *et al.* [12] and Hooshyar *et al.* [11] explain unusual fault signatures from IBRs that cause distance relays to trip incorrectly— relays tend to miss faults in their zone and

trip for faults outside their zone. Hooshyar *et al.* [13] and Haddadi *et al.* [14] show how the existing directional elements are impacted by the negative sequence current blocking feature in the inverters. Similarly, the authors in [14] and [15] illustrate how unusual fault characteristics from IBRs cause the FID schemes in existing numerical distance relays to misoperate. Our work mainly focuses on the directional elements and how the unusual fault behavior from IBRs impacts their performance.

Before the advent of numerical relays, non-numerical relays that include electromechanical and solid-state relays used phase measurements of input voltages and currents for the identification of the direction fault current. In electromechanical relay, direction is determined by measuring electrical torque generated from the input voltage and current by selecting appropriate voltage and current inputs to the relay. In solid-state relays same concept is implemented using logic gates. Directional elements have evolved with the commercialization of numerical relays. With the advancement in relay technology, the processing power of numerical relays has increased, enabling the modern relays to extract sequence components of the voltage and current measurements to decide the direction of fault current. Negative sequence component-based directional elements commonly known as $67Q$ or $67NEG$ are extensively used in numerical distance relays.

Control design of IBRs implements negative sequence current blocking functionality; this has been backed up with experimental fault data from commercial PV inverters in [8]. In systems fed by SGs, the negative sequence circuit is highly inductive, and the negative sequence voltage is expected to lag the negative sequence current by an angle around 90°. However, when the same system is fed by an IBR without any standardized fault response, we cannot expect to have the same angular characteristics. Studies carried out by Hooshyar *et al.* [13] and Haddadi *et al.* [14] illustrate how negative sequence current curtailment in inverters changes the expected angu-

lar relationship between negative sequence voltage and current during faults. This creates a severe problem for existing numerical distance relays that employ negative sequence based directional elements. These elements fail to pick up due to very small magnitudes of negative sequence fault currents; even if they pick up, they operate incorrectly due to the changed angular relationships. It is therefore essential to find a solution to tackle this problem.

1.3 Distance protection with IBRs literature review

There have been numerous efforts to address the impact of IBRs on distance relays in general. Existing works that focus on the IBR-compatible protection schemes are primarily focused on the inverter side of the problem. These schemes tend to modify the fault characteristics of the inverter so that existing distance relays can cope with them. Azzouz *et al.* [15, 16] have proposed new dual current controllers that enable the regulation of relative angles between sequence currents from IBRs during unbalanced faults to emulate the angular characteristics of SG. The control mechanisms proposed in these papers are effective for asymmetrical faults as they try to emulate the behavior of SG in a negative sequence circuit. A new formulation for impedance calculation with modified relay characteristics is proposed in [17], but it requires communication between two ends. Fang *et al.* [12] have proposed a distance protection scheme that is supervised by zero-sequence overcurrent element for unbalanced ground faults. This scheme would not work in the absence of zero sequence currents for line-to-line faults. Mishra *et al.* [18] have presented an adaptive distance relaying mechanism for distribution lines that dynamically adjusts the tripping boundary. This method controls the inverter to mimic the positive and negative sequence equiv-

alent circuit of an SG during fault. Although it talks about adaptively changing the tripping boundary, it does not shed light on the FID schemes and directional elements associated with the distance relays.

Few works are available in the existing literature that focuses on the solution to the impacts of IBRs on negative sequence based directional elements of distance relays. In [19] the authors have proposed a comprehensive dual current control scheme that modifies the angular characteristics of negative sequence voltage and current from the inverter so that they can work with existing distance relays. Also, in [13] a new directional element that uses superimposed negative sequence impedance for unbalanced faults and superimposed positive sequence impedance for balanced faults is proposed for microgrid applications. It relies on the control schemes of IBRs to calculate the superimposed impedance based on which the tripping boundary of the directional element is decided. These solutions focusing on the directional aspect of distance relays are also control-based like those above. These methods propose altering the control scheme of the inverter to attain desired fault characteristics for the existing distance relays to work. However, inverters are owned by third parties; their designs are proprietary and beyond the reach of the utilities. Thus, most of the control-based solutions are impractical.

Undoubtedly, there is a need for a more general control-agnostic and practical solution to address the impact of IBRs on distance relays caused by the failure of negative sequence component-based directional elements. This work exactly addresses these requirements by bringing forward the method used in the directional elements of non-numerical relays that is based on phase measurements, to solve the problems faced by negative sequence component-based directional elements in numerical distance relays in presence of IBRs.

1.4 Organization of thesis

Chapter 2 of the thesis focuses on the modeling and control of a grid-following inverter that implements the characteristics of commercially available inverters used by industries. After modeling the inverter, the details on the working of both numerical and non-numerical distance relays are illustrated in chapter 3. These relays are tested in a transmission level test system consisting of the inverter, SG, transmission lines, and loads, set up in PSCAD/EMTDC simulation environment. Details of the test system are described in chapter 4. Once the system is set up, different faults are simulated at various locations on the transmission line. Both relays are tested for their directionality and their performance is compared under both sources— SG and IBR— under different test scenarios. The results of the test simulations are presented in chapter 5. Ultimately, these results are analyzed to see if the directional elements in non-numerical relays can perform better than the modern relays in the presence of IBR. Chapter 6 summarizes the work carried out in the thesis with a conclusion.

Chapter 2

Inverter Modeling and Control

2.1 Overview of the model

The inverter model used in this work is a grid-following inverter with a rated power of 100 MVA at 15 kV. Under steady-state, the inverter is required to supply a rated power at unity power factor (pf). However, during faults, the power factor angle of the output current will be changed according to the FRT requirements to provide voltage support to the grid by injecting reactive power.

2.2 Control system

The control diagram for the inverter is shown in Figure 2.1. The inverter measures voltage and current output at the point of common coupling (PCC). Using a phase-locked loop (PLL), the angle reference (θ) for the reference frame conversion is extracted from the voltage measurement at the grid side. These measurements of voltage and current are then used to calculate real power output P_{out} and reactive

power Q_{out} from the inverter along with the positive sequence component of the voltage V_P. These calculated values, along with the active power setpoint— P_{set} and the pre-fault reactive power output from the inverter $Q_{prefault}$ are fed to the current reference generator that generates current reference values in dq reference frame that are used by the positive and negative sequence current control loops.

The schematic diagram for the current reference generator is shown in Figure 2.2. This is the modification of the control block in [20] to implement the FRT requirements as specified in Siemens-Gamesa [21] for grid-following inverters to provide voltage support. This control scheme allows the inverter to have a different power output range depending on whether the inverter is operating under normal or faulted conditions.

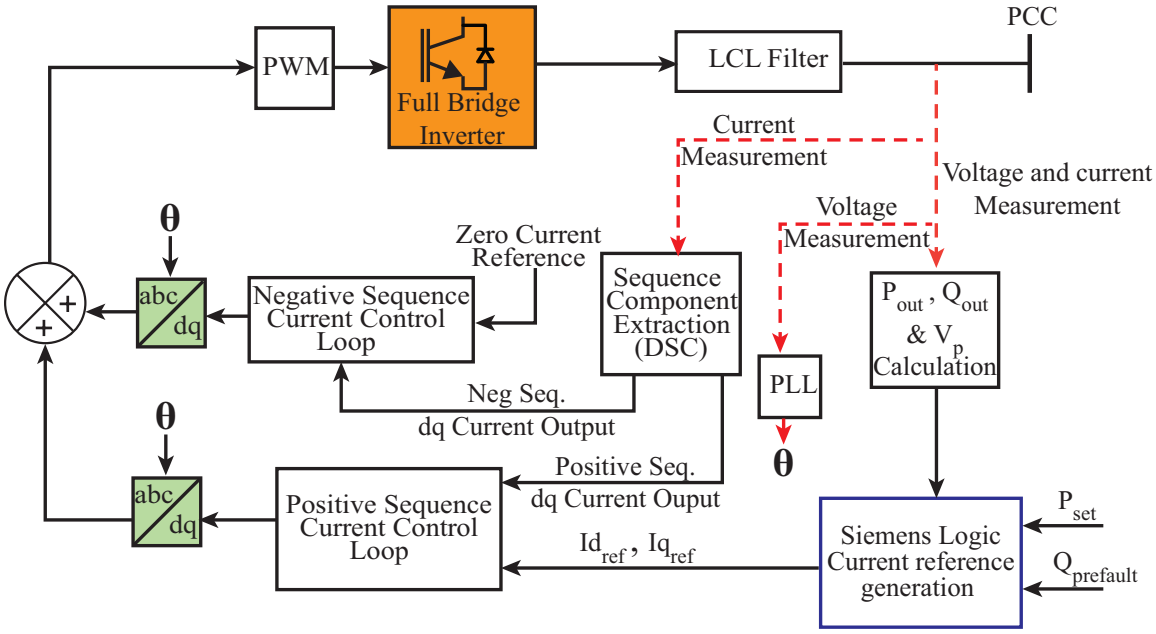

Figure 2.1: Overall control schematic of the inverter model.

2.2.1 Normal operating condition

Under normal operating conditions, i.e., when the terminal voltage V_P is between 0.9 pu and 1.1 pu, the output of the comparator is zero, and hence the active and reactive

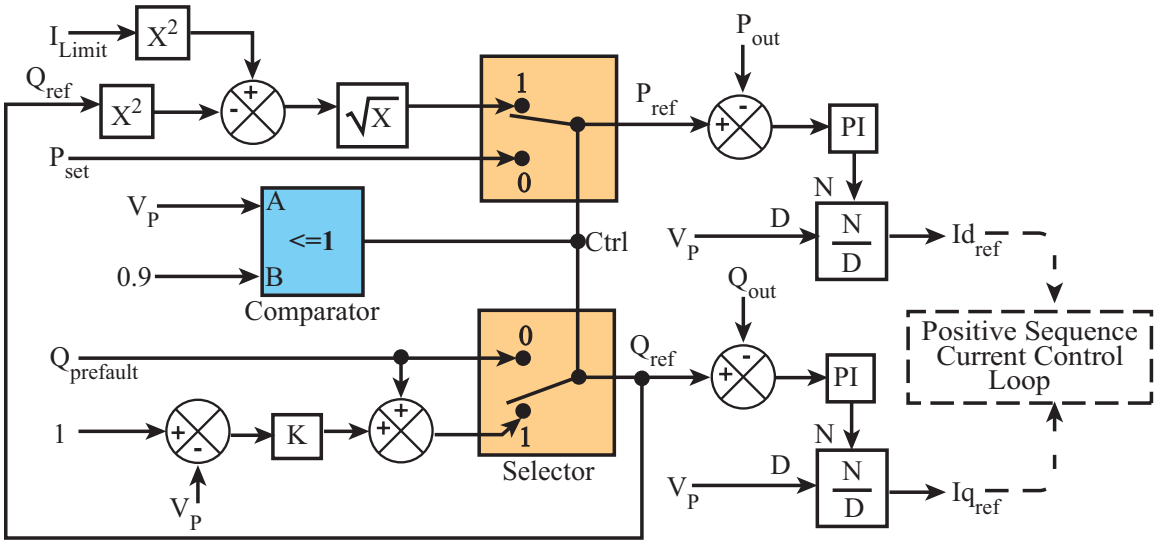

Figure 2.2: Siemens-Gamesa control logic for FRT implementation.

power references are set to P_{set} and $Q_{prefault}$ respectively as seen in Figure 2.2. Since the inverter is designed to supply rated power at unity pf during steady-state, we select $Q_{prefault} = 0$ and $P_{set} = 1$ pu for normal operating condition. From the control logic, when V_P lies in the range of normal operation, the controller will determine P_{ref} = 1 pu and Q_{ref} = 0 pu. These reference powers will be used to extract reference currents that are fed to the current control loops.

2.2.2 Abnormal operating condition

When there is a fault in the system, and V_P falls below 0.9 pu, reactive power injection from the inverter is prioritized for voltage support. Depending on the magnitude of V_P, the reference reactive power that the inverter is to inject into the gird is calculated as:

$$Q_{ref} = Q_{prefault} + K(1 - V_P). \tag{2.1}$$

Where K is a multiplier between 1 and 10, it is taken as 2 for this work. Since priority is given to reactive power, Q_{ref} is calculated first. The rest of the power that is permitted by the current limit of the inverter is injected as active power. Based on this, under abnormal operating conditions, P_{ref} is calculated as:

$$P_{ref} = \sqrt{{I_{limit}}^2 - {Q_{ref}}^2} \quad \text{pu.} \tag{2.2}$$

Where, I_{limit} is the physical limit on the current that is kept to protect the power electronics components in the inverter. Typically a the value for this limit is selected between 1.1 pu to 1.5 pu. For our design I_{limit} value of 1.1 pu has been chosen. To illustrate the operation of the control scheme for FRT implementation during abnormal condition, let us consider a scenario when $V_P = 0.7$ pu, with $K = 2$ and $Q_{prefault} = 0$. From (2.1) we get $Q_{ref} = 0.6$ pu, using this value of Q_{ref} with $I_{limt} =$ 1.1 pu in (2.2) we get, $P_{ref} = 0.92$ pu. Also, if $V_P = 0.3$ pu for more severe faults, following the same procedure we get, $Q_{ref} = 1.4$ pu. Since this value is greater than 1.1 pu, Q_{ref} is set equal to the limiting value of 1.1 pu and P_{ref} is set to zero. In this way reactive power is prioritized depending upon the magnitude of the positive sequence voltage at the inverter terminal.

Equations (2.1) and (2.2) come from the implementation of the logic shown in Figure 2.2. The control logic specified in [21] is modified so that the user can provide active and reactive power setpoints to the inverter instead of the current setpoints. Although reference values of active and reactive power are provided as input to the control scheme, the controlled power outputs from the PI controllers are changed to current references Id_{ref} and Iq_{ref} respectively, based on the terminal voltage V_P. Thus, ultimately, current is being controlled. These reference currents are then fed to the positive sequence current control loop as shown in Figure 2.1. The IBR model is also provided with a negative sequence current control loop, that operates in negative

sequence current blocking mode (zero sequence currents can still be sourced by keeping the grid-side of the interconnecting transformers YG). The negative sequence current blocking scheme is taken from [20].

Measured three-phase current output from the inverter is decomposed into positive and negative sequence components using the delayed signal cancellation (DSC) method and converted to respective dq quantities to achieve positive and negative sequence current control. Both positive and negative sequence current control loops implement PI control. For the positive sequence current control, the reference values come from the control logic shown in Figure 2.2. Since we intend to block negative sequence current, the reference values for negative sequence current control are taken as zero. The negative sequence dq current outputs are compared against zero reference while the positive sequence dq output currents are compared against Id_{ref} and Iq_{ref}. Since the control logic for FRT is implemented using active and reactive power instead of currents, the current outputs Id_{ref} and Iq_{ref} may not be within the limits of 1.1 pu. Therefore, current limiter is provided in the positive sequence current control loop so that the resultant sum of dq axis reference currents is within the limit of 1.1 pu. The limited dq reference current are are then used to synthesize the voltage reference in dq reference frame— Vd_{ref} and Vq_{ref}. These reference voltages in dq frame are converted to abc reference frame and the summation of the abc quantities from both the positive and negative sequence controllers provides the reference signal for the pulse width modulation (PWM) scheme that generates the required switching signals. The switching signals are fed to the six switches of the three-phase two-level inverter that outputs the desired voltage output. Voltage and current output from the inverter contain switching harmonics. These harmonics are filtered out from the output of the inverter using an LCL filter before connecting to the grid.

Chapter 3

Distance Relays

Distance relays are extensively used in transmission line protection as they are not affected by changing system networks and generation sources when compared to over-current relays [22]. Distance relays compare voltages and current inputs to determine the impedance to the fault and the direction of the fault. Distance elements in distance relays create impedance-plane, determine the positive sequence impedance to the fault and make the trip decision based on whether the measured impedance is within the trip zone of the relay or not. Table 3.1 summarizes how each of the distance element calculates this impedance. Notice that six elements are provided, three each for phase and ground faults. For each element, voltage and current inputs are carefully chosen such that the ratio of input voltage to current yields the positive sequence impedance to the fault. In the table, I_0 is the zero sequence component of the input current at the relay terminal, and K is the zero sequence compensation factor calculated using the zero sequence impedance Z_0 and positive sequence impedance Z_1 per unit length of the line that the relay is protecting.

Both non-numerical relays (that include electromechanical and solid-state relays) and microprocessor-based modern numerical relays use the same logic as shown in Table

Table 3.1: Distance relay units and their inputs

	Relay Units	Input Voltage	Input Current	Faults For Which The Relay Unit Operates
Ground Relays	AG	V_A	$I_A + KI_0$	AG, ABG, CAG, ABCG
	BG	V_B	$I_B + KI_0$	BG, ABG, BCG, ABCG
	CG	V_B	$I_C + KI_0$	CG, CAG, BCG, ABCG
Phase Relays	AB	$V_A - V_B$	$I_A - I_B$	AB, ABG, ABCG
	BC	$V_B - V_C$	$I_B - I_C$	BC, BCG, ABCG
	CA	$V_C - V_A$	$I_C - I_A$	CA, CAG, ABCG
Where, $K = Z_0/Z_1 - 1$				

3.1 for their distance elements. However, the implementation of the logic differs for each type of relay.

Distance elements are often implemented as mho circles and are also known as mho elements. Although these elements appear directional by nature, they require some supervision from directional elements to ensure security for certain fault conditions. Field experiences have shown that the zero sequence currents due to reverse phase-ground fault in one phase can cause the incorrect tripping of forward-reaching ground distance elements of the other phases [23]. Therefore, every distance element is equipped with some form of directional security using directional elements. The basic working of a directional element is based on the use of phase displacement between input voltages and currents to identify the direction of the fault current. There are different techniques by which the direction of fault is identified. Older non-numerical relays use the displacement between actual phasor measurements of input voltages and currents, whereas modern microprocessor-based relays use the phase angle dis-

placement between negative sequence component of the voltage and current inputs to the relay. The working principles of directional elements in both non-numerical and numerical distance relays are illustrated in the following sections.

3.1 Non-numerical distance relays

Directional elements in electromechanical and solid-state distance relays identify the direction of the fault current by comparing the phase angle between input phase voltages and phase currents. Electromechanical relays make the trip decision based on the measure of the electrical torque developed that changes with the angular displacement between voltage and current. Solid-state relays use the same principle, but they use logic gates for the implementation. Therefore, instead of physical torque, a digital trip signal is generated. Voltage and current inputs to the relay are carefully chosen to maximize the operating torque produced in the relay coils during faults. The Choice of voltage and current inputs and their connection is essential because different faults involving different phases exhibit different angular relationships between the input voltage and current. It is desired that a connection works reliably under different fault scenarios.

One of the most widely used relay connections in the directional elements used in non-numerical relays is the 90° - 30° directional element [9], where there is a 90° angle between polarizing (reference) voltage and the current given to each phase relay coil. The working of phase a element of the directional element is shown in Figure 3.1. In figure, I_a is the input current and V_{bc} is the input voltage (reference voltage). Notice that the input voltage is carefully chosen to be in quadrature with the input current by selecting the voltages of the other two phases. This ensures the availability of sufficient voltage V_{bc} for the relay to operate even when there is a bolted phase to

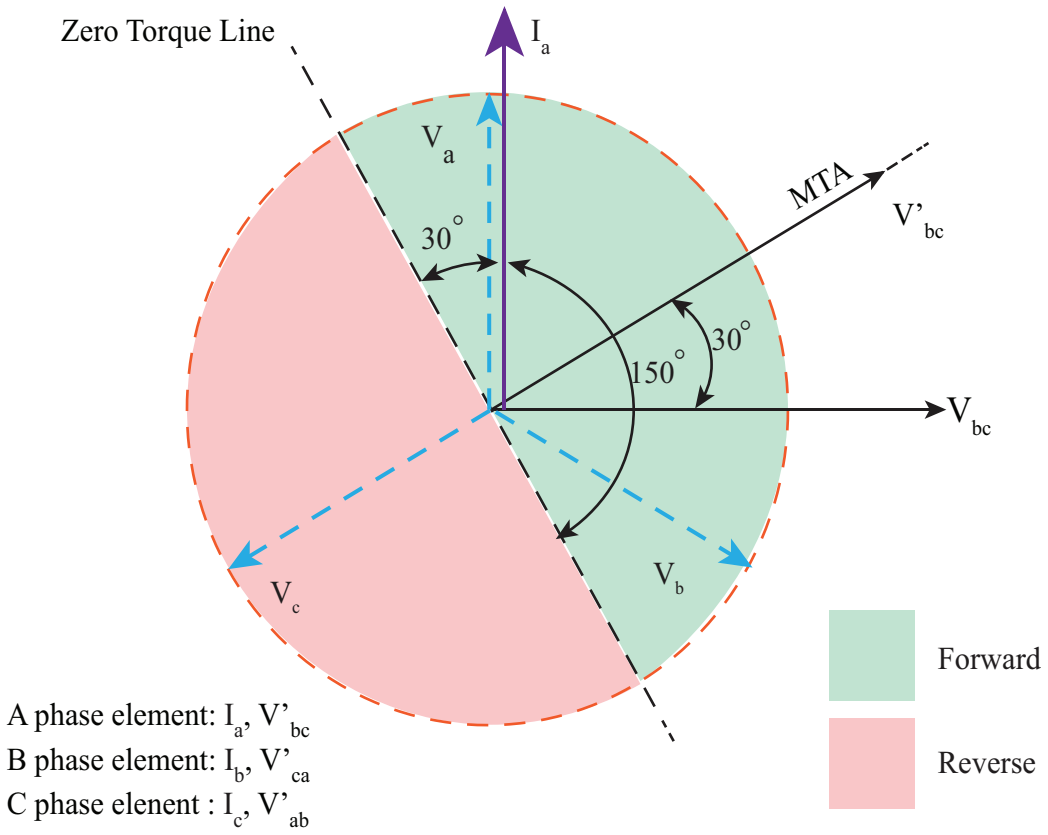

Figure 3.1: Working principle of 90° - 30° directional element.

ground fault in phase a. Fault currents are highly lagging due to the inductive nature of the transmission system; this makes the fault current I_a lag its pre-fault value. It is desirable that the input voltage is almost in phase with this lagging current during faults for maximum torque. Based on this physics of the fault, the input voltage is further skewed in an anti-clockwise direction by a certain angle so that the voltage comes closer to the current I_a, during faults. This angle is a user setting, which is typically between 30° and 90°, known as Maximum Torque Angle (MTA). MTA for the design shown in Figure 3.1 is 30°. Skewed V_{bc} is denoted in the figure as V'_{bc} and is known as the polarizing voltage or the reference voltage. Similar design procedures are taken for the elements in the other two phases, b and c, by replacing current I_a and voltage V_{bc} with their respective measurements as shown in Figure 3.1.

A trip decision is made by each directional element based on the comparison of the phase angle between the input current and the polarizing voltage. During a fault, if the input current (I_a for phase A element) lies within $\pm 90^\circ$ from the polarizing voltage (V'_{bc}), the relay interprets the fault as forward. The relay interprets the fault as reverse, otherwise. Forward zone of the phase A element of the 90° - 30° directional relay is shown by the green region in Figure 3.1. The reverse zone is shaded in red.

3.2 Numerical distance relays

Numerical relays are equipped with microprocessors that enable them to process the input voltages/currents and extract more information about the system. This information is used to detect and diagnose unusual system events like faults. For example, numerical relays can obtain the sequence components out of the input phase voltages and currents, and extensively use these components for fault detection and supervision. One of the most commonly used features in numerical distance relays is the negative sequence component-based directional element, also known as $67Q$ or $67NEG$, which assists distance relays with identifying the direction of fault current.

Negative sequence component-based directional elements used in numerical distance relays compare the angle between the negative sequence voltage V_2 and current I_2 by calculating the negative sequence impedance, Z_2 (V_2/I_2) at the relay terminal. The phase angle of Z_2 is what decides the direction of the fault. To illustrate this concept, let us consider a negative sequence circuit of a transmission system as shown in Figure 3.2, where the transmission line is fed by two systems X and Y with equivalent impedances of ZSX_2 and ZSY_2 respectively.

In the circuit shown in Figure 3.2, for the forward fault as shown, KVL from system

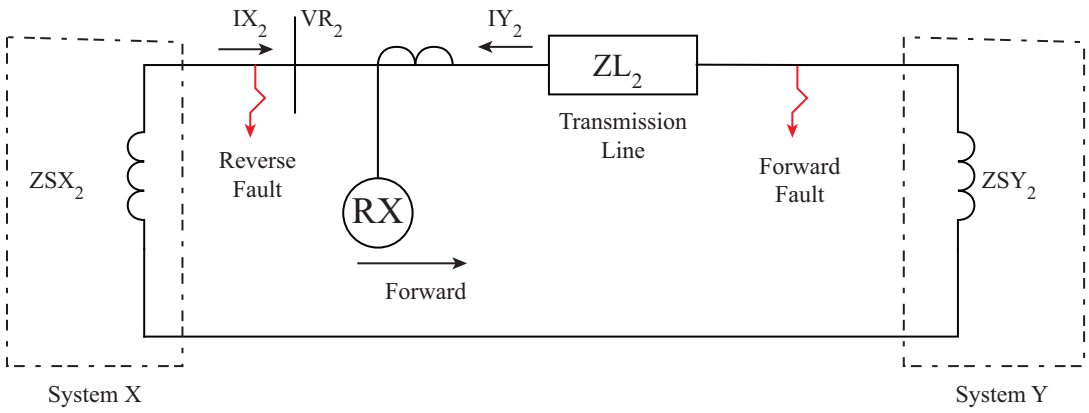

Figure 3.2: Negative sequence circuit of a transmission system.

X to the relay terminal is given by:

$$VX_2 - IX_2 \,.\, ZSX_2 = VR_2. \tag{3.1}$$

Here, VR_2 is the negative sequence voltage measured at the relay terminal and IX_2 is the negative sequence current seen by the relay for a forward fault. We can assume the negative sequence voltage at remote system X— VX_2 to be zero. This implies that the negative sequence impedance seen by the relay from (3.1) can be given by,

$$Z_{2F} = \frac{VR_2}{IX_2} = -ZSX_2. \tag{3.2}$$

However, for a reverse fault, we can write KVL from the relay terminal to System Y as,

$$VSY_2 - IY_2 \,.\, ZL_2 - IY_2 \,.\, ZSY_2 = VR_2 \tag{3.3}$$

we can assume VSY_2 to be zero for the same reason as it was for VSX_2. Then, the

above equation can be written as,

$$VR_2 = -IY_2(ZL_2 + ZSY_2) \tag{3.4}$$

The relay has CT connections set for forward faults; for reverse fault currents it measures the current with 180° phase shift. Therefore, the negative sequence impedance measured by the relay for reverse faults is given by,

$$Z_{2R} = \frac{VR_2}{IY_2\angle 180^\circ} = ZSY_2 + ZL_2. \tag{3.5}$$

Here, $IY_2\angle 180^\circ$ is the actual current measured by the relay during a reverse fault. These relationships follow simply from the application of KVL in the negative sequence circuit. For a transmission system, the equivalent negative sequence impedance ZSX_2 and ZSY_2 consist of the negative sequence impedance of SG, transformer, and transmission lines for each system, all of which are highly inductive. This suggests that the angle of Z_{2F} in (3.2) is around -90° and that of Z_{2R} in (3.5) is around $+90^\circ$.

Based on this Physics of the negative sequence circuit, the angular positions of different negative sequence impedance measured by the relay can be shown in R-X plane as in Figure 3.3. It can be seen that for a typical transmission system, there is approximately a 180° phase difference in Z_2 for faults in forward and reverse direction, i.e., forward/reverse fault results in approximately $-90^\circ/+90^\circ$ angle of Z_2 as mentioned earlier. This property is used by the $67Q$ element to identify forward and reverse faults.

A graphical representation of forward and reverse zones of the 67Q element is also shown in Fig. 3.3. The value of MTA is a user setting that determines the forward/reverse phase angles to enable the relay decision. In general, MTA is chosen as the angle of the protected line's negative sequence impedance (same as the positive

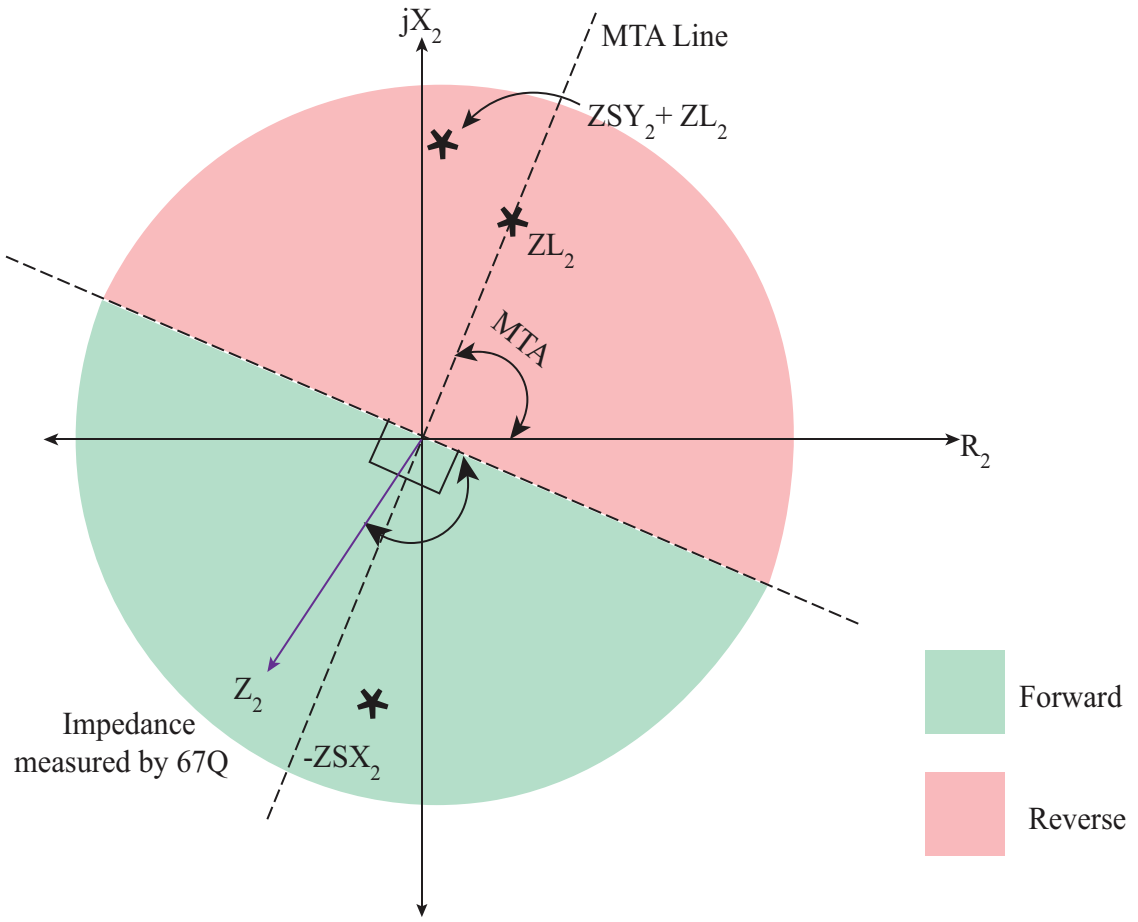

Figure 3.3: Working principle of 67Q directional element.

sequence impedance), ZL_2. Since forward faults cause the angle of Z_2 to be around $-90°$, to decide fault direction, the MTA line is extended backward, and the angular position of Z_2 is compared with the extended line. If Z_2 is within a range of $\pm 90°$ from the extended MTA line, the fault is declared as forward; otherwise, the fault is declared as reverse.

Chapter 4

Simulation Test System

The simulation test system is a two-bus 230 kV transmission system with sources connected to each bus. A schematic diagram of the test system is shown in Figure 4.1, where two SGs are connected to bus 1 and bus 2. Distance relay is placed at bus 1, protecting the transmission line. A constant PQ load of 135 MVA load with 0.9 pf lagging is placed at bus 2.

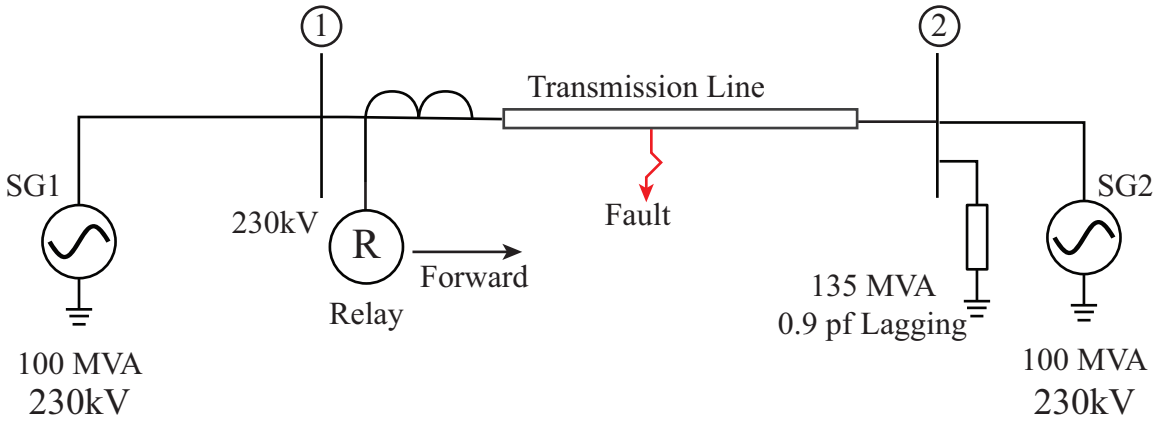

Figure 4.1: Simulation test system with SG behind the distance relay.

4.1 Transmission line

The 150 km long transmission line is rated at 100 MVA, 230 kV. The line is modeled with distributed parameters using Bergeron Model in PSCAD/EMTDC. The equivalent parameters of the transmission line used in the simulation are as follows:

$$R_1 = 4.4965 \times 10^{-5}\ \Omega/m$$

$$XL_1 = 2.5509 \times 10^{-4}\ \Omega/m$$

$$XC_1 = 355.1\ M\Omega * m$$

$$R_0 = 1.1241 \times 10^{-4}\ \Omega/m$$

$$XL_0 = 5.2885 \times 10^{-4}\ \Omega/m$$

$$XC_0 = 603.68\ M\Omega * m$$

4.2 Synchronous generators

Two SGs as shown in Figure 4.1, each rated at 100 MVA, 230kV are modeled as Thevenin equivalent sources. The parameters for the two SGs used in the simulation model are as follows:

SG1

$Zs_1 = 79.35\angle 80^\circ\ \Omega$

$Zs_0 = 23.81\angle 80^\circ\ \Omega$

$\delta = 10^\circ$

SG2

$Zs_1 = 74.86\angle 82^\circ\ \Omega$

$Zs_0 = 22.46\angle 82^\circ\ \Omega$

$\delta = 0^\circ$

4.3 IBR

The IBR model as explained in chapter 2 is modeled in PSCAD and implemented in the test system as shown in Figure 4.2. The inverter is rated at 100 MVA, 15 kV, and connects to the transmission line via a 100 MVA 15 kV/230 kV transformer. The transformer has a positive sequence leakage reactance of 0.01 pu.

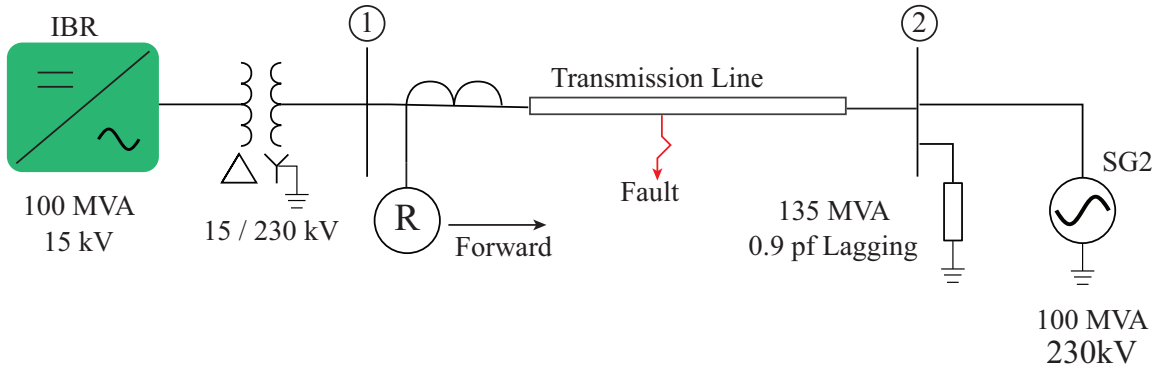

Figure 4.2: Simulation test system with an IBR behind the distance relay.

4.4 Distance relays

Two distance relays— non-numerical and numerical distance relays— explained in chapter 3 are placed in bus 1 protecting the line 1-2. For the non-numerical relay an electromechanical relay with 90° - 30° directional element is taken. This relay is tested against a numerical relay with negative sequence component-based directional element 67Q. The performance of these two directional elements is compared in presence of both SG and IBR behind them for different faults in the transmission line.

Chapter 5

Results and Discussion

As discussed in chapter 3, the method by which the distance elements in both numerical and non-numerical distance relays determine the impedance of the faulted portion of the line is the same. However, the methods used by directional elements differ in the two relays. Thus, the performance of negative sequence based directional element— $67Q$, in numerical relays is tested against the 90° - 30° directional element in non-numerical relays in the test system described in chapter 4 with appropriate input voltages and currents fed to the relays. As the negative sequence based directional element $67Q$ does not operate for balanced faults, the performance of two relays is compared by simulating unbalanced faults only. The polarizing voltage and input current for each phase of the 90° - 30° directional element is provided as shown in Fig. 3.1. Also, for the 67Q element, MTA is chosen as 80°, which is also the line's negative/positive sequence impedance angle. The decision for direction made by the relays is determined as explained in chapter 3 for each relay. Different units of distance relay are also implemented using Table 3.1. Since the method used by distance elements in numerical and non-numerical relays is the same, impedance measured by only one of the distance elements is presented for all the test cases and compared

against the actual impedance of the faulted section of the line. All Simulations are performed in PSCAD/EMTDC environment.

5.1 Fault characteristics of inverter model

As discussed already, the inverter model is designed to implement FRT characteristics that prioritize reactive power injection during faults depending on the magnitude of positive sequence voltage at the inverter terminal. To illustrate this, two unbalanced faults, line-to-ground (LG) and line-to-line-to-ground (LLG) faults, are simulated at a distance of 75 km from the relay in the transmission line as shown in Figure 4.2. The performance of the developed IBR model under these faults is shown in Figure 5.1 and 5.2. Fault starts at 1 s into the simulation. From the current output, we can see that for both faults, the fault currents are limited to 1.1 pu (peak of pre-fault instantaneous currents is taken as the base). Due to the implementation of the negative sequence current blocking control scheme the negative sequence current output (I^-) during fault is zero. Also, the zero sequence current (I^0) is zero during the fault, resulting in a purely positive sequence current output. It is important to notice that these outputs are at the inverter terminal. Therefore I^0 is zero even for unbalanced ground faults. However, on the high voltage side, zero sequence currents sourced by the high-side Y grounded transformer do exist during both faults.

As the magnitude of V_P decreases from 0.6 pu during AG fault to around 0.25 pu during BCG fault, the active power output from the inverter drops from around 0.5 pu to zero. This operation is consistent with (2.1), which shows that a lower value of V_P requires a higher share of reactive power output. At $V_P = 0.25$ pu, the reactive power output according to (2.1) is around 1.75 pu, which demands a current output higher than the current limit of 1.1 pu. Therefore, for a limiting value of output

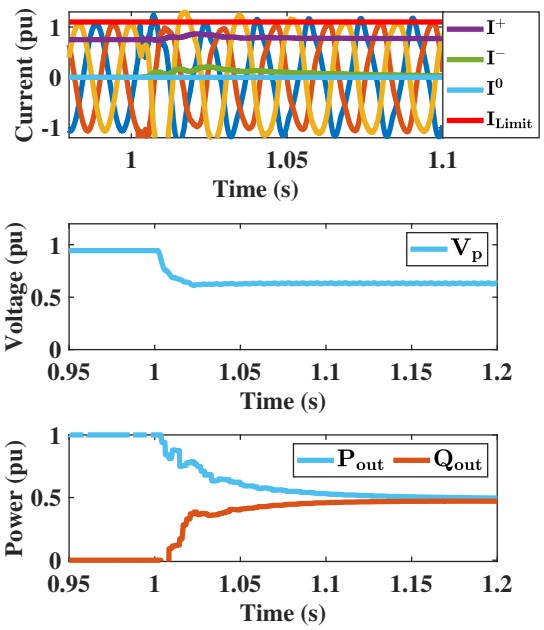

Figure 5.1: IBR performance for an AG fault.

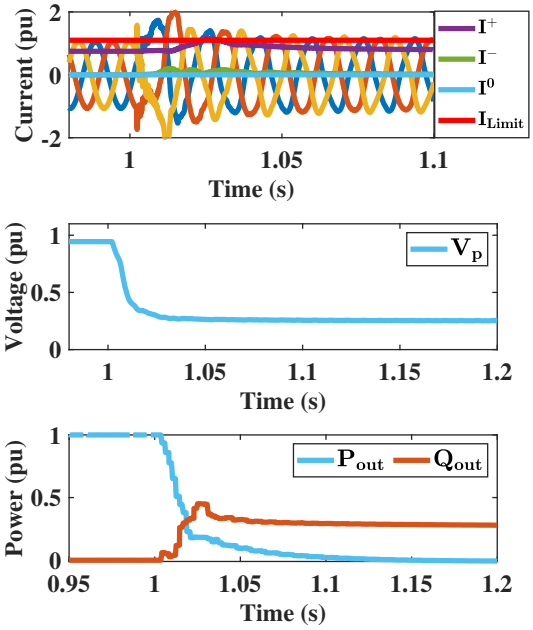

Figure 5.2: IBR performance for a BCG fault.

reactive current at 1.1 pu, the power output of the inverter is around 0.3 pu and is purely reactive. This shows the correct implementation of the FRT characteristics and the control features as shown in Figure 2.2 and Figure 2.1.

5.2 Performance of relays when fed by SG

With a SG feeding the relay as shown in Figure 4.1, all three unbalanced faults— LG, line-to-line (LL), and LLG with negligible fault resistance of 0.001 Ω are simulated on the line at three different locations of 15 km, 75 km, and 135 km. Numerical relay with 67Q directional element and an electromechanical (non-numerical) relay with 90° - 30° directional elements are placed in bus 1 one after another with CT connections such that they measure the current flowing from bus 1 to bus 2 as positive.

For an AG fault simulated in the line at a distance of 75 km from the relay, the angular positions of V_2, I_2 and Z_2 during the fault as recorded by the 67Q directional element are pictorially represented in Figure 5.3. We can see that V_2 lags I_2 by an angle of around 100° and Z_2 measured by the relay lies within the forward zone, correctly indicating a forward fault. Similarly, in Figure 5.4, for the 90° - 30° element, the input current I_a is almost in phase with the polarizing voltage V'_{bc}. Since the input current lies within ±90° from the polarizing voltage, the relay correctly identifies the direction of the fault as forward. For other faults simulated at different locations, the angular position of the polarizing voltage and input current, along with the decision made by the relays, are summarized in Table 5.1. The impedance to fault measured by the distance elements of the two relays (since both relays use the same method, impedance measured by them is the same) for all test cases are also presented in the table. With a SG feeding the relays, the results show that both the relays correctly identify the direction of all faults as forward (F). This is expected because both relays are designed based on the physics of the fault fed by a SG. The behavior of a SG during faults is standardized and predictable. Also, the impedance values measured by the distance elements are very close to the actual impedance of the faulted section of the line indicating that for each scenario the distance elements of both relays are performing as expected. Hence, the distance relays when fed by SG are able to accurately determine both distance and direction of the fault.

5.3 Performance of relays when fed by IBR

With the SG behind the relay replaced by a grid-following inverter, the relays are again tested for the same faults. For the same AG fault in the line at a distance of 75 km from the relay, Figure 5.5 shows how the IBR control design brings the

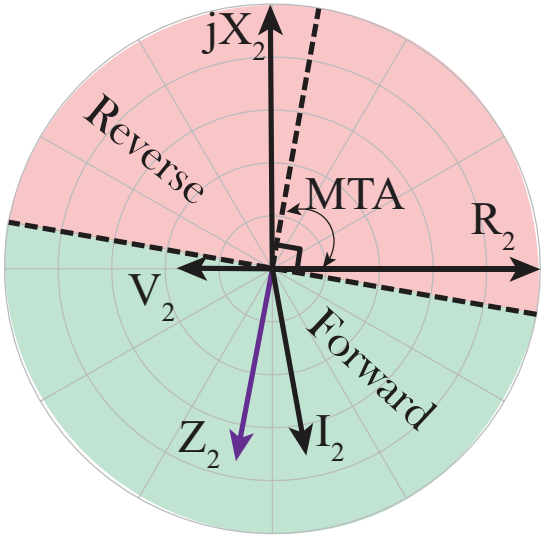

Figure 5.3: Recording by a numerical relay during an AG fault fed by a SG.

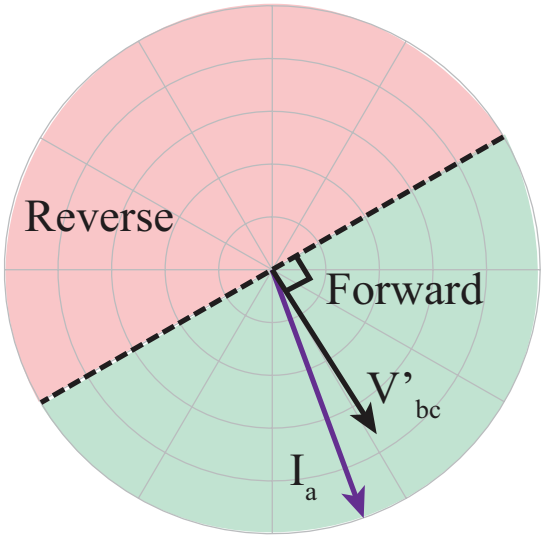

Figure 5.4: Recording by an electromechanical relay during an AG fault fed by a SG.

magnitude of I_2, which was near 2 pu when fed by SG, to zero. With IBR designed to block negative sequence current, the magnitude of I_2 two cycles into the fault is less than 0.1 pu. With this small magnitude, the 67Q element fails to pick up with its typical pickup setting of 0.2 pu. However, to observe what direction the relay gives if it were to operate, the pickup setting is reduced to 0.02 pu. With this new setting, the relay picks up but fails to identify the correct direction of the fault as depicted in Figure 5.6, where the voltage V_2 is leading I_2 by an angle of 42°, causing the impedance measured by the relay Z_2 to be in the reverse zone of the relay. The relay misoperates, identifying a forward fault as reverse. The control design of IBR implementing power factor control not only limits the magnitude of I_2 but also changes the angular relationship between V_2 and I_2. These changed angular positions do not follow the expected trend as in the highly inductive negative sequence circuit of a SG where V_2 lags I_2 by an angle close to 90°. This causes the 67Q directional element that looks for a standard angular relationship between V_2 and I_2 to fail in the presence of IBRs.

Table 5.1: Comparison of the performance of relays with SG

Fault Distance (km)	*Fault Type*	$90° - 30°$ *Element*		*67Q Element*		*Distance Element*		*Directional Element*	
		Element	$\angle V_{pol}$ - $\angle I$ *(deg)*	$\lvert I_2 \rvert$ (pu)	$\angle V_2 - \angle I_2$ *(deg)*	*Actual Z1* (Ω)	*Calculated Z1* (Ω)	$90° - 30°$	*67Q*
15	AG	A	14	2.42	-100.35	0.674+ j3.826	0.686 + j3.832	F	F
	BC	B	12.57	3.04	-99.5		0.681 + j3.842	F	F
	BCG	C	-28.6	1.55	-98.71		0.677 + j3.843	F	F
75	BG	B	13	1.9	-99.64	3.372 + j19.132	3.38 + j19.15	F	F
	CA	C	6.95	2.5	-100.67		3.41 + j19.17	F	F
	CAG	A	-13.14	1.42	-101.4		3.41 + j19.14	F	F
135	CG	C	12	1.7	-99.83	6.070 + j34.437	6.11 + j34.59	F	F
	AB	A	4.06	2.2	-100.4		6.12 + j34.58	F	F
	ABG	B	-1.3	1.14	-100.84		6.12 + j34.58	F	F

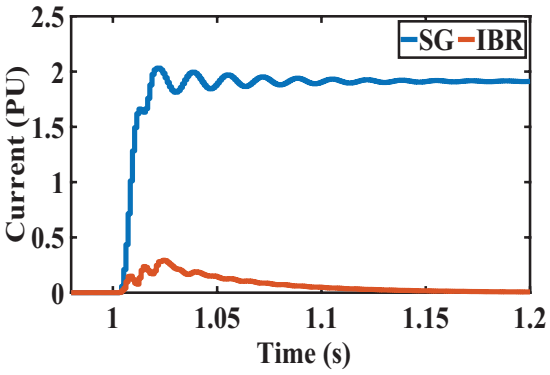

Figure 5.5: Magnitude of negative sequence currents during an AG fault with different sources.

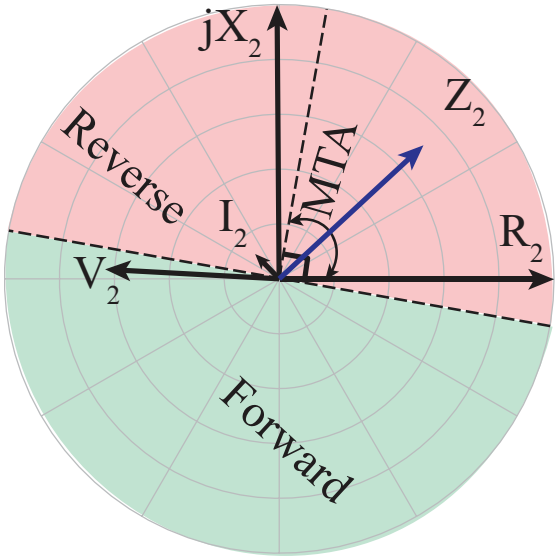

Figure 5.6: Recording by a numerical relay during an AG fault fed by an IBR.

For the same scenario, with the numerical relay implementing the 67Q directional element replaced by an electromechanical relay with 90° - 30° element, the relay is able to correctly identify the direction of the fault as shown in Figure 5.7, where the input current I_a for phase a element of the relay is within 2° from the polarizing voltage V'_{bc} and lies in the forward zone of the relay. The relay thus correctly identifies the fault as a forward fault. Since the 90° - 30° directional element uses only phase measurements instead of negative sequence components for its decision, it is immune to the IBR control action blocking negative sequence currents. Although IBR control brings I_2 to zero, the phase current I_a is still significant (around 2.5 pu for IBR with Δ - YG transformer and 1.1 pu for IBR with Y-Δ transformer) as seen in Figure 5.8 during the fault, for the relay to operate. Comparing Figure 5.4 with Figure 5.7, it can be seen that the angular relationship between the input phase current to the relay and the polarizing voltage is still preserved even when the source feeding the 90° - 30° directional element is changed from a SG to an IBR. This enables the relay to work consistently irrespective of the source feeding it, unlike numerical relays.

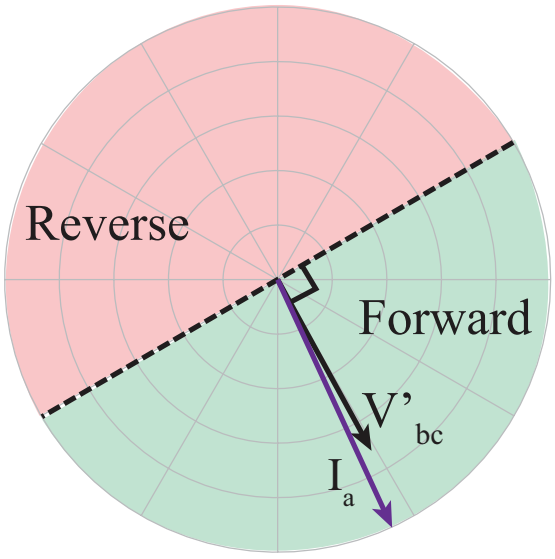

Figure 5.7: Recording by an electromechanical relay during an AG fault fed by an IBR.

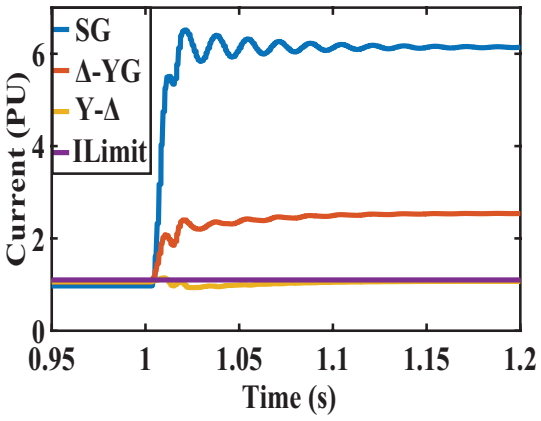

Figure 5.8: Phase a current magnitude during an AG fault with different sources

Table 5.2: Comparison of the performance of relays with IBRs

Fault Distance (km)	***Trans-former***	***Fault Type***	$90° - 30°$ ***Element***		***67Q Element***		***Distance Element***		***Directional Element***	
			Relay Unit	$\angle \mathbf{V_{pol}}$ - $\angle \mathbf{I}$ ***(deg)***	$\lvert \mathbf{I_2} \rvert$ ***(pu)***	$\angle \mathbf{V_2} - \angle \mathbf{I_2}$ ***(deg)***	***Actual Z1*** (Ω)	***Calculated Z1*** (Ω)	$90° - 30°$	***67Q***
15	Δ-YG	AG	A	7.89	0.081	32.76	0.674+ j3.826	0.675 + j3.83	F	R
		BC	B	38.9	0.067	17.35		0.7 + j3.82	F	R
		BCG	C	-54	0.021	40.5		0.68 + j3.83	F	R
	Y-Δ	AG	A	-30	0.057	39.6		0.686 + j3.81	F	R
		BC	B	41.56	0.07	25.1		0.642 + j3.82	F	R
		BCG	C	-5.94	0.055	35.45		0.649 + j3.78	F	R
75	Δ-YG	BG	B	3.01	0.067	34.93	3.372 + j19.132	3.39 + j19.06	F	R
		CA	C	21.5	0.08	34		3.37 + j19.15	F	R
		CAG	A	-48.9	0.033	22.3		3.33 + j18.84	F	R
	Y-Δ	BG	B	-28.4	0.057	38.3		3.35 + j19.1	F	R
		CA	C	21.51	0.082	33.9		3.49 + j19.07	F	R
		CAG	A	-4.41	0.05	25.32		3.36 + j19.11	F	R
135	Δ-YG	CG	C	-4.22	0.07	35.25	6.070 + j34.437	6.13 + j34.67	F	R
		AB	A	18.1	0.08	35.2		6.21 + j34.61	F	R
		ABG	B	-37.7	0.04	28.8		5.86 + j34.45	F	R
	Y-Δ	CG	C	-25.6	0.065	36.7		6.08 + j34.57	F	R
		AB	A	18.1	0.08	35.2		6.13 + j34.36	F	R
		ABG	B	-2.5	0.046	24.33		5.98 + j34.58	F	R

For other faults simulated at different locations in the line with relays fed by IBR, the results are shown in Table 5.2. Simulations are performed with two different configurations of the interconnecting transformer: Δ-YG and Y(ungrounded)-Δ. It can be seen that for all the simulated fault scenarios, the numerical relay with 67Q directional element misidentifies the forward fault as reverse (R). However, the $90^\circ - 30^\circ$ element correctly identifies all the faults as forward faults. The results show that the directional elements for non-numerical relays that use phase measurements instead of negative sequence measurements can still be used accurately in the presence of IBRs. Also, it is important to note that the impedance to fault values — $Z1$, measured by the distance elements of the two distance relays, for all simulation test cases even with IBR feeding the relays are very close to the actual impedance of the faulted section of the line. Simulation results in Table 5.1 and Table 5.2 show that the method for distance elements discussed in chapter 3 works accurately irrespective of the source feeding the distance relays. Therefore, addressing the misoperations of negative sequence component-based directional elements in numerical distance relays by replacing them with the phase component-based directional elements, the performance of numerical distance relays can be enhanced in the presence of IBRs.

Chapter 6

Conclusion

This work highlights the challenges that distance relays face in the presence of inverter-based resources and investigates the performance of distance and directional elements of distance relays used in both non-numerical distance relays and numerical distance relays. Distance elements used in both relays are shown to be unaffected by the presence of IBRs. However, the directional element used in numerical distance relays fails to determine the correct direction of the fault current in the presence of IBRs. A thorough analysis is carried out on the misoperations of negative sequence component-based directional elements used in numerical distance relays. A solution is proposed to address this misoperation by replacing the negative sequence component-based method in numerical distance relays with phase quantities-based method used in non-numerical distance relays. The concepts and working principles of both directional elements are illustrated, and the performance of both relays are individually scrutinized and compared with each other, first with the relays fed by a SG and then by an IBR.

The negative sequence component-based directional element $67Q$ used in modern numerical distance relays works accurately, as expected when fed by a SG. However,

the relay misoperates, identifying forward faults as reverse when fed by an IBR. The phase quantities-based 90° - 30° directional element used in non-numerical distance relays, on the other hand, operates correctly for all faults, including the ones for which the 67Q directional element fails. The phase quantities-based method can be easily implemented in microprocessor-equipped numerical relays. Thus, misoperations of numerical distance relays that occur due to the incorrect identification of fault direction can be addressed using the phase quantities-based method to identify fault direction instead of the negative sequence component-based method.

Bibliography

[1] Claire Stockwell et al. *Climate summit momentum: Paris commitments improved warming estimate to 2.4°C*. Tech. rep. Climate Analytics, NewClimate Institute, May 2021. URL: https://climateactiontracker.org/documents/853/CAT_2021-05-04_Briefing_Global-Update_Climate-Summit-Momentum.pdf.

[2] Anne Sjoerd Brouwer et al. "Operational flexibility and economics of power plants in future low-carbon power systems". In: *Applied Energy* 156 (2015), pp. 107–128. ISSN: 0306-2619. DOI: https://doi.org/10.1016/j.apenergy.2015.06.065. URL: https://www.sciencedirect.com/science/article/pii/S0306261915008235.

[3] Galen L. Barbose. *U.S. Renewables Portfolio Standards 2021 Annual Status Update: Early Release*. Tech. rep. Lawrence Berkeley National Laboratory, Feb. 2021. URL: https://emp.lbl.gov/projects/renewables-portfolio/.

[4] EIA. *Annual Energy Outlook 2021*. Tech. rep. U.S. Energy Information Administration, Feb. 2021. URL: https://www.eia.gov/outlooks/aeo/.

[5] Abdullah Alshahrani et al. "The Technical Challenges Facing the Integration of Small-Scale and Large-scale PV Systems into the Grid: A Critical Review". In: *Electronics* 8.12 (2019). ISSN: 2079-9292. DOI: 10.3390/electronics8121443. URL: https://www.mdpi.com/2079-9292/8/12/1443.

[6] A. Morales et al. "Advanced grid requirements for the integration of wind farms into the Spanish transmission system". In: *IET Renew. Power Gen* 2.1 (Mar. 2008), pp. 47–59.

[7] *Technical Requirements for the Connection and Operation of Customer Installations to the Extra High Voltage Network (TAR Extra High Voltage)*. Tech. rep. VDE-AR-N 4130. VDE VERLAG, 2018. URL: https://bit.ly/3autC4h.

[8] S. Gonzalez et al. "Fault Current Experimental Results of Photovoltaic Inverters Operating with Grid-Support Functionality". In: *2018 IEEE 7th World Conference on Photovoltaic Energy Conversion (WCPEC) (A Joint Conference of 45th IEEE PVSC, 28th PVSEC 34th EU PVSEC)*. 2018, pp. 1406–1411. DOI: 10.1109/PVSC.2018.8547449.

[9] J. L. Blackburn and T. J. Domin. *Protective Relaying: Principles and Applications*. 3rd ed. Boca Raton, FL, USA: CRC Press, 2006.

[10] Mukesh Nagpal and Charles Henville. "Impact of Power-Electronic Sources on Transmission Line Ground Fault Protection". In: *IEEE Transactions on Power Delivery* 33.1 (2018), pp. 62–70. DOI: 10.1109/TPWRD.2017.2709279.

[11] A. Hooshyar, M. A. Azzouz, and E. F. El-Saadany. "Distance Protection of Lines Emanating From Full-Scale Converter-Interfaced Renewable Energy Power Plants—Part I: Problem Statement". In: *IEEE Transactions on Power Delivery* 30.4 (2015), pp. 1770–1780. DOI: 10.1109/TPWRD.2014.2369479.

[12] Y. Fang et al. "Impact of Inverter-Interfaced Renewable Energy Generators on Distance Protection and an Improved Scheme". In: *IEEE Transactions on Industrial Electronics* 66.9 (2019), pp. 7078–7088. DOI: 10.1109/TIE.2018.2873521.

[13] A. Hooshyar and R. Iravani. "A New Directional Element for Microgrid Protection". In: *IEEE Transactions on Smart Grid* 9.6 (2018), pp. 6862–6876. DOI: 10.1109/TSG.2017.2727400.

[14] A. Haddadi et al. "Impact of Inverter-Based Resources on Negative Sequence Quantities-Based Protection Elements". In: *IEEE Transactions on Power Delivery* 36.1 (2021), pp. 289–298. DOI: 10.1109/TPWRD.2020.2978075.

[15] M. A. Azzouz, A. Hooshyar, and E. F. El-Saadany. "Resilience Enhancement of Microgrids With Inverter-Interfaced DGs by Enabling Faulty Phase Selection". In: *IEEE Transactions on Smart Grid* 9.6 (2018), pp. 6578–6589. DOI: 10.1109/TSG.2017.2716342.

[16] Maher A. Azzouz and Ali Hooshyar. "Dual Current Control of Inverter-Interfaced Renewable Energy Sources for Precise Phase Selection". In: *IEEE Transactions on Smart Grid* 10.5 (2019), pp. 5092–5102. DOI: 10.1109/TSG.2018.2875422.

[17] A. Hooshyar, M. A. Azzouz, and E. F. El-Saadany. "Distance Protection of Lines Emanating From Full-Scale Converter-Interfaced Renewable Energy Power Plants—Part II: Solution Description and Evaluation". In: *IEEE Transactions on Power Delivery* 30.4 (2015), pp. 1781–1791. DOI: 10.1109/TPWRD.2014.2369480.

[18] P. Mishra, A. K. Pradhan, and P. Bajpai. "Adaptive Distance Relaying for Distribution Lines Connecting Inverter-Interfaced Solar PV Plant". In: *IEEE Transactions on Industrial Electronics* 68.3 (2021), pp. 2300–2309. DOI: 10.1109/TIE.2020.2975462.

[19] Amin Banaiemoqadam, Ali Hooshyar, and Maher Abdelkhalek Azzouz. "A Comprehensive Dual Current Control Scheme for Inverter-Based Resources to Enable Correct Operation of Protective Relays". In: *IEEE Transactions on Power Delivery* (2020), pp. 1–1. DOI: 10.1109/TPWRD.2020.3025878.

[20] Phani Harsha Gadde and Sukumar Brahma. "Realistic Microgrid Test Bed for Protection and Resiliency Studies". In: *2019 North American Power Symposium (NAPS)*. 2019, pp. 1–6. DOI: 10.1109/NAPS46351.2019.9000214.

[21] *Modification of Commercial Fault Calculation Program for Wind Turbine Generators*. Report PES-TR78. IEEE Power & Energy Society, 2020.

[22] Paul M. Anderson. "Transmission Protection". In: *Power System Protection*. 1999, pp. 377–377. DOI: 10.1109/9780470545591.part3.

[23] Edmund O. Schweitzer, III and Jeff Roberts. "Distance Relay Element Design". In: *SEL Journal of Reliable Power*. Vol. 1. 1. 2010, pp. 4–14.